




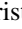





**Orbital localization and the role of the Fe and As 4*p* orbitals in BaFe<sub>2</sub>As<sub>2</sub> probed by XANES**

A. G. de Figueiredo <sup>1</sup>, M. R. Cantarino <sup>1</sup>, W. R. da Silva Neto <sup>1,2</sup>, K. R. Pakuszewski <sup>3</sup>, R. Grossi <sup>3</sup>,  
D. S. Christovam <sup>3,\*</sup>, J. C. Souza <sup>3</sup>, M. M. Piva <sup>3,\*</sup>, G. S. Freitas<sup>3</sup>, P. G. Pagliuso<sup>3</sup>, C. Adriano<sup>3</sup> and F. A. Garcia <sup>1,†</sup>

<sup>1</sup>Instituto de Física, Universidade de São Paulo, São Paulo-São Paulo 05508-090, Brazil

<sup>2</sup>Instituto de Química, Universidade de São Paulo, São Paulo-São Paulo 05508-090, Brazil

<sup>3</sup>Inst Fis Gleb Wataghin, Universidade Estadual de Campinas, Campinas-São Paulo 13083-859, Brazil



(Received 21 October 2021; revised 18 December 2021; accepted 6 January 2022; published 21 January 2022)

The polarization dependence of the near edge x-ray absorption spectroscopy (XANES) is an element specific probe to the real-space distribution of the density of unoccupied states in solid-state materials. In this paper, we present Fe and As *K*-edge experiments of Ba(Fe<sub>1-*x*</sub>M<sub>*x*</sub>)<sub>2</sub>As<sub>2</sub> (*M* = Mn, Co, and *x* = 0.0 and 0.08). The experiments reveal a strong polarization dependence of the probed XANES spectra, which concerns mainly an increase in the intensity of electronic transitions when the beam polarization is set out of the sample's *ab* crystallographic plane. The results show that states with *p<sub>z</sub>*-orbital character dominate the density of unoccupied states close to the Fermi level. Partial substitution of Fe by Co is shown to decrease the intensity anisotropy, suggesting that Co promotes electronic transfer preferentially to states with *p<sub>z</sub>*-orbital character. On the other hand, Mn substitution causes the increase in the spectra *p<sub>z</sub>*-orbital anisotropy, which is proposed to take place by means of an enhanced local Fe 3*d*4*p* mixing, unveiling the role of Fe 4*p* states in the localization of the Fe 3*d* orbitals. Moreover, by comparing our results to previous experiments, we identify the relative mixing between Fe and pnictide 4*p<sub>x,y,z</sub>* orbitals as a clear divide between the electronic properties of iron arsenides and selenides. Our conclusions are supported by multiple-scattering theory calculations of the XANES spectra and by quantum chemistry calculations of the Fe coordination electronic structure.

DOI: [10.1103/PhysRevB.105.045130](https://doi.org/10.1103/PhysRevB.105.045130)

**I. INTRODUCTION**

Doping an electronic correlated phase often results in rich phase diagrams containing regions dominated by strong electronic correlations and other regions wherein Fermi-liquid behavior is observed. The relatively recently introduced Fe pnictide (FePn) materials [1] denote a large family of high-temperature unconventional superconducting materials that seems to lie on the border between weak and strong electronic correlations [2]. Indeed, the description of the relevant electronic degrees of freedom in terms of either localized or itinerant states underlines a major conceptual divide in this field [3–6].

The 122 parent compound BaFe<sub>2</sub>As<sub>2</sub> is a particularly well-explored FePn material. Phases derived from the partial substitution of Fe by Co, Ba(Fe<sub>1-*x*</sub>Co<sub>*x*</sub>)<sub>2</sub>As<sub>2</sub>, is a much debated subject mainly because it leads to a robust and clean superconducting (SC) ground state [2,7]. In the case of Ba(Fe<sub>1-*x*</sub>Mn<sub>*x*</sub>)<sub>2</sub>As<sub>2</sub>, however, no SC phase is observed [8]. In principle, partial substitution at the Fe site by Mn pushes the BaFe<sub>2</sub>As<sub>2</sub> electronic properties to a Mott region, whereas partial substitution by Co tends to decrease its electronic correlations. Indeed, the end points of the Ba(Fe<sub>1-*x*</sub>M<sub>*x*</sub>)<sub>2</sub>As<sub>2</sub> (*M* = Mn or Co) materials, BaMn<sub>2</sub>As<sub>2</sub> and BaCo<sub>2</sub>As<sub>2</sub>, are

characterized as an antiferromagnetic Mott insulator [9,10] and a weakly correlated metal [11,12], respectively, somehow corroborating the proposed substitutional trends.

The BaFe<sub>2</sub>As<sub>2</sub> structure features FeAs layers well spaced by Ba<sup>2+</sup> cations where Fe is fourfold coordinated by As atoms arranged in a slightly distorted tetrahedral geometry. This structure breaks the degeneracy of the Fe derived 3*d* states close to the Fermi level, directly affecting the BaFe<sub>2</sub>As<sub>2</sub> Fermi-surface composition, making the Fe coordination an important parameter to understanding the 122 materials electronic properties [2]. In this paper, we focus precisely on the electronic properties of the FeAs coordination complex, investigating the polarization and composition dependencies of the near edge (XANES) Fe and As *K*-edge x-ray absorption spectra (XAS) of Ba(Fe<sub>1-*x*</sub>M<sub>*x*</sub>)<sub>2</sub>As<sub>2</sub> (*M* = Mn or Co, *x* = 0.0, and *x* = 0.08) single crystals.

Hard XAS experiments could provide a handful of key information to the field of the FePns materials, including the role of transition-metal substitution on their electronic [13–18] and structural properties [19–24] as well as the degree of electronic correlations [18,25–27] in these systems. Here, we take advantage of the dipole selection rules dependence on the beam polarization that makes the XAS spectra strongly angular dependent. Focusing on the XANES region of the XAS spectra, we, thus, probe, in real space, the distribution of the density of unoccupied electronic states in our materials.

For all investigated materials, our results suggest that the density of unoccupied states at Fermi level has a predominant *p<sub>z</sub>*-orbital character, in agreement with the case of the

\*Present address: Max Planck Institute for Chemical Physics of Solids, Nöthnitzer Straße 40, 01187 Dresden, Germany.

†Corresponding author: fgarcia@if.usp.br

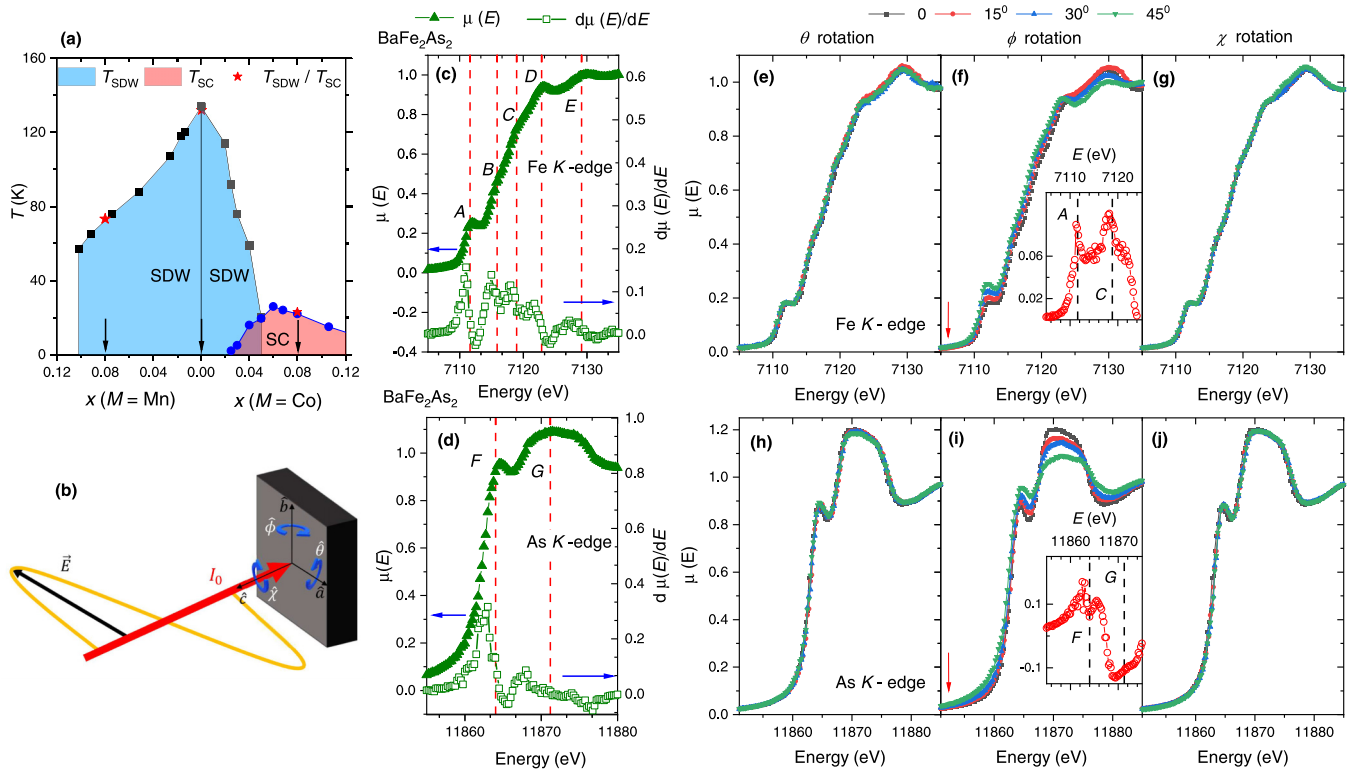


FIG. 1. (a) Composition ( $x$ ) vs  $T$  phase diagram for the  $\text{Ba}(\text{Fe}_{1-x}\text{Mn}_x)_2\text{As}_2$  and  $\text{Ba}(\text{Fe}_{1-x}\text{Co}_x)_2\text{As}_2$  transition-metal substituted iron arsenides (black squares are data from Ref. [35]). (b) Schematic of the experimental geometry, defining the rotation angles  $\phi$ ,  $\theta$ , and  $\chi$  as rotations around the  $a$ ,  $b$ , and  $c$  axes, respectively. (c) Representative  $\text{BaFe}_2\text{As}_2$  Fe  $K$ -edge normalized XANES spectrum [ $\mu(E)$ , left axis, full symbols] and its derivative [ $d\mu(E)/dE$ , right axis, open symbols]. Capital letters A–E mark the transitions, and the dashed lines associate the features in the spectrum derivative to the spectrum. (d) The respective As  $K$ -edge data of  $\text{BaFe}_2\text{As}_2$  with capital letters F and G labeling the absorption features (e)–(j). Polarization dependence of the Fe  $K$ -edge and As  $K$ -edge XANES spectra of  $\text{BaFe}_2\text{As}_2$ . The open red circles in the insets of panels (f) and (i) show the difference spectrum [ $\mu(E)_{\phi=45^\circ} - \mu(E)_{\phi=0^\circ}$ ] with the dashed lines marking some representative energy positions.

iron arsenide  $\text{SmFeAsO}$  [28]. Co substitution is shown to populate preferentially the As  $4p_z$  orbitals, characterizing a distinct charge-transfer anisotropy. Mn substitution increases the spectra  $p_z$ -orbital anisotropy suggesting the localization of the Fe  $3d$  and As  $4p$  states, adding yet another piece of evidence that the  $\text{BaFe}_2\text{As}_2$  material can be tuned to a correlated electronic phase [25] but this time not by doping. From our calculations and experiments, we conclude that the  $\text{BaFe}_2\text{As}_2$  electronic structure displays a delicate interplay between the local Fe  $3d4p$  mixing and the metal-to-ligand Fe  $3d$  As  $4p$  mixing. Our findings unveil the role of the Fe  $4p$  states and allow one to make a clear distinction between the iron arsenides and the iron selenides for which the unoccupied states were found to have a predominant Se  $4p_{x,y}$  character [29].

Our experiments are analyzed based on two complementary frameworks. We first present multiple-scattering theory calculations (as implemented by the FEFF8.4 code [30,31]) where we found relative agreement between our calculations and experiments for the Fe  $K$  edge and As  $K$  edge. Nevertheless, FEFF is not able to capture the angular dependence of the probed spectra. Then, we present multiconfigurational electronic structure calculations of the orbital states of a single  $\text{FeAs}_4$  coordination complex as implemented by ORCA 5.0 [32,33].

## II. MATERIAL AND METHODS

$\text{Ba}(\text{Fe}_{1-x}\text{M}_x)_2\text{As}_2$  ( $M = \text{Mn}$  or  $\text{Co}$ ,  $x = 0.0$  or  $0.08$ ) single crystals were synthesized by an In-flux technique as described in Ref. [34]. The Laue patterns of all samples were obtained to determine the relative orientation of the  $a$  and  $b$  crystallographic axes. A composition ( $x$ ) vs temperature ( $T$ ) phase diagram of Mn and Co substituted samples is presented in Fig. 1(a) for context. Black squares and blue circles mark the data from Ref. [35], and red stars mark the data for our samples as determined from resistivity measurements [34,36,37]. The investigated samples are indicated by black arrows.

The Fe  $K$ -edge and As  $K$ -edge hard XAS experiments were performed at the XDS beamline [38] of the Brazilian Synchrotron Light Source (CNPEM-LNLS) at room temperature. Data were acquired by the partial Fe and As fluorescence. The samples were mounted in a Huber 6 + 2-circle diffractometer with the experimental geometry as explained in Fig. 1(b). The beam polarization direction is fixed and is aligned to one of the sample crystallographic axes, which will be hereafter called the  $a$  axis. XANES spectra were, thus, collected for rotations about the in-plane  $a$  and  $b$  axes and the out-of-plane  $c$  axis which are, respectively, termed  $\theta$ ,  $\phi$ , and  $\chi$  rotations [see Fig. 1(b)]. For all rotations, we adopted an angular ( $\alpha$ ) interval of  $0 < \alpha < 45^\circ$ . All spectra were normalized in ATHENA [39].

FEFF calculations [31] were adopted to calculate the XANES spectra. The *ab initio* calculations were performed and converged for clusters of up to 282 atoms for the Fe *K* edge and 144 atoms for the As *K* edge. In both cases, the Hedin-Lundqvist [40] pseudopotential was adopted to account for the effect of the local exchange correlation. Self-consistent calculations were performed for a cluster radius of 6.5 Å (Fe *K* edge) and 8.0 Å (As *K* edge). Quadrupolar transitions and spin-orbit coupling effects were considered, but no sizeable effects were observed. Chemical substitution effects were simulated in the case of the As *K* edge by substituting one in ten Fe atoms by one Mn (Co) atom. The large self-consistent 8-Å radius was adopted to include all dopants in the self-consistent calculations.

Multiconfigurational electronic calculations of the electronic states of a FeAs<sub>4</sub> tetrahedral-like molecule were implemented by ORCA 5.0 [32,33]. Ionic charges were set as  $-3$  for each arsenic ion and  $+2$  for the metallic center, resulting in a  $S = 2$  molecule, consistent with a high spin complex within tetrahedral-like coordination ( $D_{2d}$  symmetry). Atomic positions were obtained from the BaFe<sub>2</sub>As<sub>2</sub> crystallographic data.

To capture the optimized configuration of the electronic states in this 3*d*-metal complex, we apply the complete active space- (CAS-) self-consistent field method, and electronic correlations were later taken into account by *n*-electron valence state perturbation theory (NEVPT-2) calculations. The relativistic adapted Karlsruhe valence triple- $\zeta$  with two sets of polarization functions were adopted as the basis set within the ZORA approximation [41]. We built a CAS consisting only of the five 3*d* orbitals and its six electrons—CAS(6,5)—in the  $D_{2d}$  symmetry, and the ligand field parameters were obtained at the end of the calculation. Virtual states, 5 eV above the Fermi level, were calculated similarly but adopting a CAS(2,12) [42].

### III. RESULTS AND DISCUSSION

In Figs. 1(c) and 1(d), we present representative normalized [ $\mu(E)$ ] Fe and As *K*-edge spectra of BaFe<sub>2</sub>As<sub>2</sub> along with their respective spectra derivatives. The Fe *K*-edge XANES spectrum presents five absorption features labeled by capital letters *A–E*. The features are positioned in the midrange between the maxima and the minima of the spectrum derivative. Features *A–C* are of electronic nature, whereas features *D* and *E* are predominantly due to scattering processes [13–15]. The *A* feature sits at about  $E_F$ , which is found to be  $E_F \approx 7111.6$  eV. This feature is called the preedge and is understood to stem from a dipolar transition from the Fe 1*s* to Fe 3*d* As 4*p* hybrid bands. It comprises a series of energy levels located in a 1- to 2-eV bandwidth about  $E_F$  and expresses the properties of the FeAs tetrahedral coordination complex. Feature *B* denote transitions to hybrid states (including Fe 4*s* and As 4*p* states) lying 3 eV above the Fe 3*d* As 4*p* states. Feature *C*, at about  $\approx 7118.6$  eV, is the main atomic transition of the Fe *K* edge and stems from Fe 1*s*  $\rightarrow$  4*p* transitions [43,44].

The As *K*-edge XANES spectrum in Fig. 1(d) displays two main features, which we called *F* and *G*. The former identify

the main As 1*s*  $\rightarrow$  4*p* atomic electronic transition which, due to the As coordination, also includes contributions from Fe 3*d* orbitals. The latter is mainly due to scattering processes and transitions to excited electronic states 5 eV above  $E_F$ . The *F* feature sits about  $E_F \approx 11864.3$  eV.

In Figs. 1(e)–1(g), we present the Fe *K*-edge spectra of BaFe<sub>2</sub>As<sub>2</sub> for all investigated rotations. In its local coordinate frame, rotating the sample is equivalent to changing the incident beam polarization, which leads to new selection rules for the dipole transitions. A  $\theta$  rotation is, thus, a control experiment, which does not change the beam polarization. Indeed, a direct inspection of Fig. 1(e) reveals that  $\theta$  rotations do not change the spectra. A  $\chi$  rotation probes orbitals with planar components (as the  $p_x$  and  $p_y$  orbitals) whereas  $\phi$  rotations probe orbitals with  $z$  symmetry as  $p_z$  orbitals.

The preedge intensities of the observed spectra clearly increase under  $\phi$  rotations [Fig. 1(f)] characterizing the spectra anisotropy. The inset in Fig. 1(f) displays the difference spectrum, obtained from making  $\mu(E, \phi = 45^\circ) - \mu(E, \phi = 0)$ . As is clear, the anisotropy is strong in the preedge (*A* feature) but persists in all the regions of the electronic transitions, peaking again close to the main edge (*C* feature). The red arrow in the figure calls attention to the fact that the baseline of the spectra coincides in the region below the  $E_F$ , excluding a systematic shift of the background signal as a source of the effect. Our analysis will focus on the electronic transitions and, in particular, in the preedge transition.

The significant increase in the preedge intensity for a  $\phi$  rotation shows that the mixing between Fe-3*d* and As-4*p<sub>z</sub>* orbitals form states with a higher density of unoccupied states than the Fe 3*d* As 4*p<sub>x,y</sub>* orbitals. The observed lack of in-plane anisotropy for a  $\chi$  rotation is expected because the  $p_x$ - and  $p_y$ -orbital symmetries are not reduced in a tetragonal environment [45]. Indeed, it is to be noted that the Fe-derived 3*d* states are observed via their hybridization with *p* states and, therefore, the *p*-state symmetries are the relevant properties in discussing the preedge polarization dependence. In addition, the very observation of the XAS polarization dependence is unexpected since in itinerant electron systems the ligands are expected to be weak due to screening by conduction electrons. These results add to the importance of the local electronic properties of itinerant magnets [46].

In Figs. 1(h)–1(j), we show the As *K*-edge spectra data. Here, one can also observe that  $\theta$  and  $\chi$  rotations do not change the spectra. Again, the spectra are clearly anisotropic for  $\phi$  rotations with the absorption edge becoming more intense. This result provides a direct assessment of the As 4*p<sub>z</sub>* relative lower electronic filling and larger anisotropic orbital character. We also call attention to the red arrow in Fig. 1(i), showing that the baseline of the spectra coincides in the region below the Fermi level. In the inset, we show the difference spectrum which evidences the large anisotropy of both *F* and *G* features.

Our next step is to investigate the composition dependence of the above effects. We start by inspecting the Fe *K* edge of Mn- and Co-substituted samples. Their XANES normalized spectra [ $\mu(E)$ ] are presented in Figs. 2(a)–2(f). The Co-substituted sample is a superconductor with  $T_{SC} \approx 22$  K whereas the Mn-rich sample does not display SC [see Fig. 1(a)]. The putative electronic effects of the Co and Mn

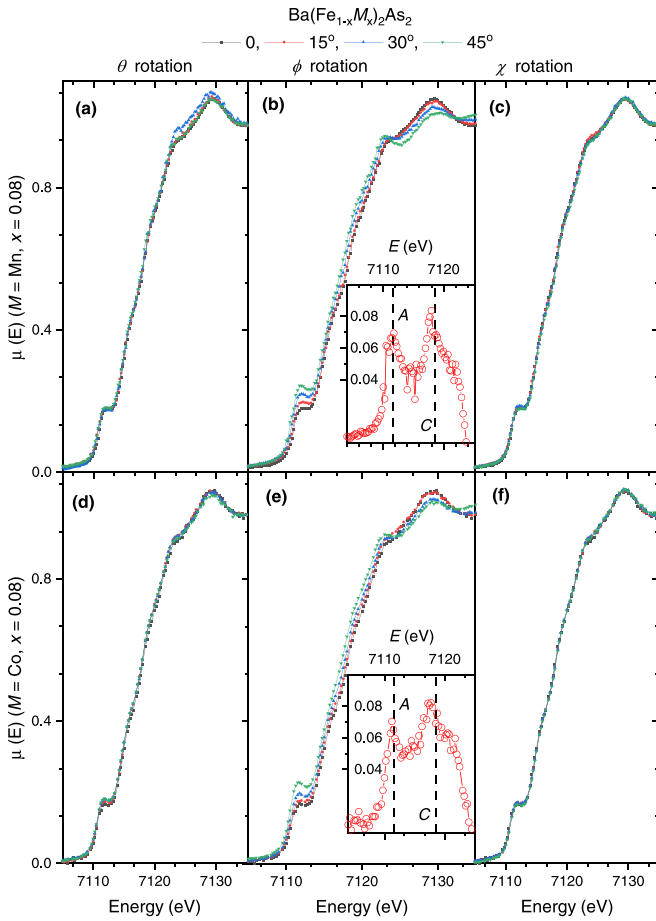


FIG. 2. Fe  $K$ -edge XANES spectra of (a)–(c)  $\text{Ba}(\text{Fe}_{1.92}\text{Mn}_{0.08})_2\text{As}_2$  and (d)–(f)  $\text{Ba}(\text{Fe}_{1.92}\text{Co}_{0.08})_2\text{As}_2$  as a function of the polarization (see figures’ top). In all cases, the normalized intensities  $[\mu(E)]$  are presented. The open red circles in the insets of panels (b) and (e) show the difference spectrum  $[\mu(E)_{\phi=45} - \mu(E)_{\phi=0}]$  with the dashed lines marking some representative energy positions.

substitutions would be symmetric with respect to hole and electron doping making these samples ideal for our studies. Concerning  $\theta$  and  $\chi$  rotations, the results are similar to what was found in the parent compound, whereas the data for  $\phi$  rotations suggest a weak composition dependency of this anisotropy.

The insets in Figs. 2(b) and 2(e) present the difference spectra for the Mn- and Co-substituted samples, respectively, and show this effect in more detail. Moreover, the  $C$  feature remains markedly anisotropic under  $\phi$  rotations, showing that Fe  $4p_z$  orbitals form bands with a higher unoccupied density of states than the Fe  $4p_{x,y}$  orbitals. This particular result for the  $\text{BaFe}_2\text{As}_2$  parent compound and doped materials is in contrast to the case of  $\text{SmFeAsO}$  [28]. In addition, as in previous XANES experiments of iron arsenides, the  $C$  feature is not much affected by Co substitution [13,14,16,17] and is here shown to be unaffected by Mn substitution as well.

The composition effect is better observed by our analysis in Figs. 3(a)–3(c). To quantify the intensities anisotropy as a function of  $\phi$ , we fit the Fe  $K$ -edge spectra by a Lorentzian

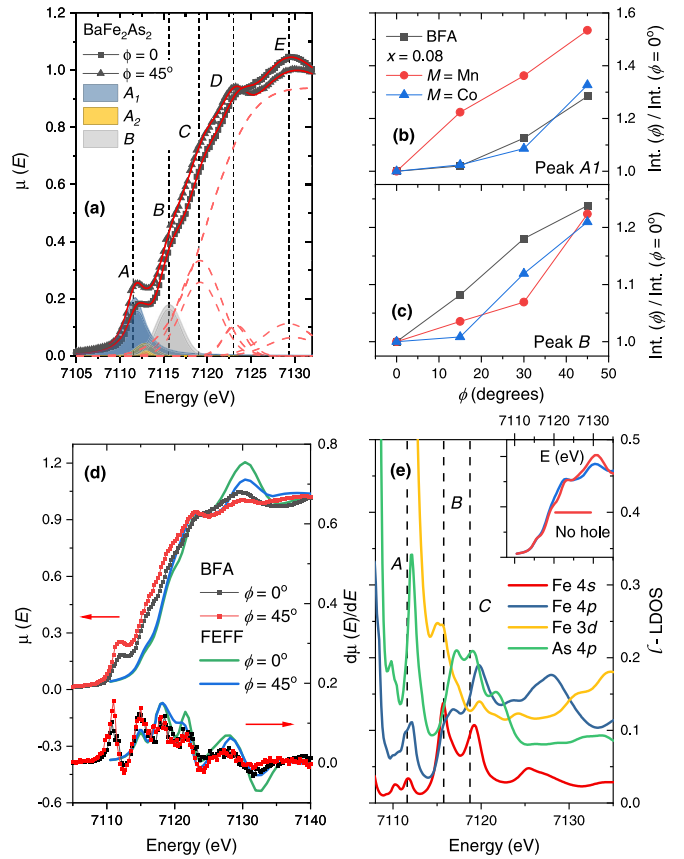


FIG. 3. (a) Fe  $K$ -edge XANES spectra of  $\text{BaFe}_2\text{As}_2$  ( $\phi = 0$  and  $\phi = 45$ ) and their respective phenomenological fittings. As shown, two peaks, termed  $A_1$  and  $A_2$ , are included to describe the pre-edge  $A$  feature. The shaded regions below the curves are the peak areas which are adopted as the resonance intensities. The intensities are presented in (b) and (c), respectively, for the  $A_1$ -pre-edge peak and the  $B$ -edge peak as a function of  $\phi$  and composition. In (d), we present polarization-dependent FEFF calculations of the Fe  $K$ -edge spectra (left axis) and its derivative (right axis) compared to the respective experimental data. A shift of  $-1.3$  eV and a broadening of 1 eV were considered in the calculations. In panel (e), we show the FEFF calculated site and orbital-projected LDOS of  $\text{BaFe}_2\text{As}_2$ . Features  $A$ ,  $B$ , and  $C$  are presented for comparison to the results. The inset of the figure compares the FEFF-calculated spectra ( $\phi = 45^\circ$ ) with and without core-hole effects.

(the  $A_1$  peaks) and Gaussian (the  $A_2$ ,  $B$ ,  $C$ ,  $D$ , and  $E$  peaks) line shapes plus a Fermi-Dirac function as in Fig. 3(a). The two peaks in the pre-edge region are clearly present in high-resolution experiments [17] and are suggested by the analysis of our spectra derivatives. Indeed, adopting two peaks is instrumental to extract a consistent fitting analysis. The resonance intensities  $I_{\text{peak}}$  are estimated from the peak areas as in the shades of Fig. 3(a).

The  $A_1$  feature sits just at  $E_F$  whereas the  $B$  feature lies  $\approx 3$  eV above it. We, thus, compare the chemical substitution electronic effects in these two distinct situations by tracking the anisotropy behavior of the  $A_1$  and  $B$  features. In Figs. 3(b) and 3(c), respectively, we plot the  $I_{A_1}$  and  $I_B$  normalized intensities as functions of  $\phi$  for the compositions as indicated. Each data set is normalized as  $I_{\text{peak}}(\phi)/I_{\text{peak}}(\phi = 0)$ .

The  $A_1$  peak of the Mn-substituted sample is distinctly more anisotropic, but the composition effect is not present in the case of the  $B$  feature. Since the latter lies  $\approx 3$  eV above  $E_F$ , it would be hardly affected by chemical substitution as observed. A naive interpretation about the effect of Mn substitution is that Mn doping fills the Fe  $3d$  As  $4p$  hybrid bands with holes, increasing the amount of unoccupied states. At the present doping level, however, Mn impurities do not act as charge dopants to  $\text{BaFe}_2\text{As}_2$  [47,48], and we will return to this discussion later by proposing a distinct mechanism for the effects of chemical substitution.

In many instances [30,31,49], FEFF calculations provide a first approach to the interpretation of the XANES spectra. In Fig. 3(d), we show polarization-dependent FEFF calculations of the  $\text{BaFe}_2\text{As}_2$  Fe  $K$ -edge spectra and their derivatives compared to experimental data. The calculations reproduce well the  $B$ – $E$  feature positions, but their polarization dependencies are not fully reproduced. Moreover, the  $A$  feature is missed completely, reflecting that FEFF calculations do not capture in full the properties of bound states [30,31,49].

If core-hole effects can be considered weak, the nature of the observed transitions can be associated with the element (site) and orbital projected local density of states (LDOS). In Fig. 3(e), we present the LDOS obtained from FEFF calculations, focusing on the Fe- and As-derived states. High densities of states are predicted at the positions of the  $A$ ,  $B$ , and  $C$  features. In particular, the  $B$  and  $C$  features correlate, respectively, to the LDOS due to the Fe  $4s$  and As and Fe  $4p$  states. As anticipated in our discussion, the  $A$  feature can be associated with a high LDOS derived from Fe- $3d$  and As- $4p$  states. In addition, our calculations also predict a high density of Fe  $4p$  states about this same region, inviting an investigation into the role of the local Fe  $3d4p$  hybridization, which we will discuss based on quantum chemistry calculations. The inset of Fig. 3(e), compares the FEFF-calculated spectra with and without core-hole effects, and the close similarity between the calculations suggests that our discussion is adequate in a first approximation.

We now turn to the As  $K$ -edge experiments of other compositions. In Figs. 4(a)–4(f), the normalized intensities  $[\mu(E)]$  of the As  $K$ -edge XANES spectra of the doped samples are presented. Again, the measured spectra are isotropic under  $\theta$  and  $\chi$  rotations. In the case of  $\phi$  rotations, however, both  $\text{Ba}(\text{Fe}_{1.92}\text{Mn}_{0.08})_2\text{As}_2$  and  $\text{Ba}(\text{Fe}_{1.92}\text{Co}_{0.08})_2\text{As}_2$  spectra are polarization dependent, but this time, the composition effect is straightforwardly observed by direct inspection of Figs. 4(b) and 4(e). The insets of the same figures present the respective difference spectrum  $[\mu(E)_{\phi=45} - \mu(E)_{\phi=0}]$ . The insets are on the same scale, making it clear that the XANES anisotropy is larger for the Mn-rich material. Moreover, it is also clear that the edge anisotropy of the Co-substituted sample decreases when compared to the case of the parent compound, whereas it increases for the Mn-containing sample. Since the As- $K$  edge is a direct probe to the properties of the As  $4p_{x,y,z}$  orbitals sitting at about  $E_F$ , the distinction between the localization and the occupation of the As  $4p_z$  orbitals should be more evident as observed.

The anisotropy of the postedge feature at about 11 870 eV, which is about 5 eV above the Fermi level, is also affected by composition, being less intense for the Co-substituted

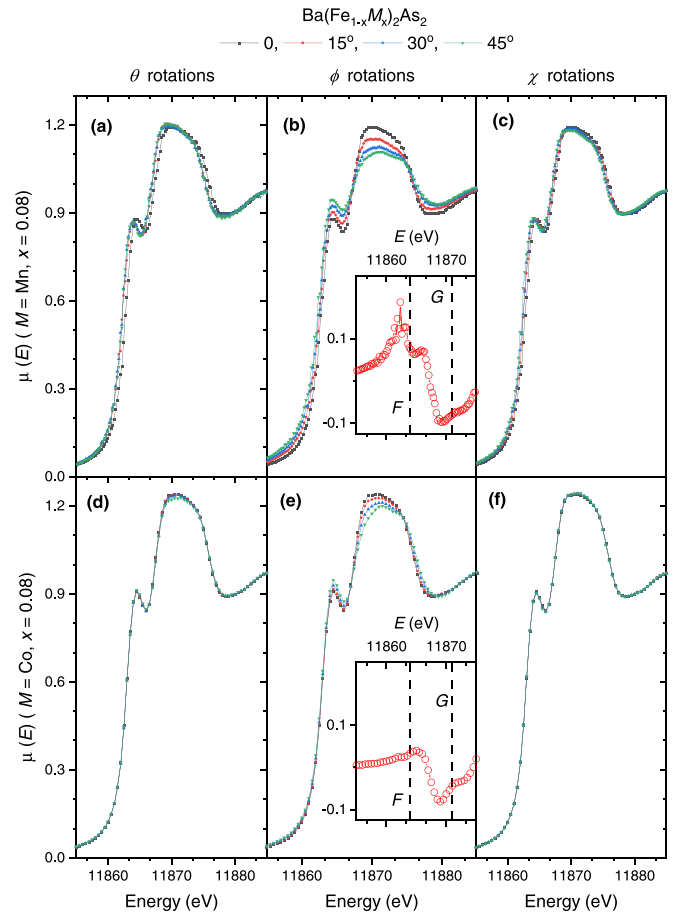


FIG. 4. As  $K$ -edge XANES spectra of (a)–(c)  $\text{Ba}(\text{Fe}_{1.92}\text{Mn}_{0.08})_2\text{As}_2$  and (d)–(f)  $\text{Ba}(\text{Fe}_{1.92}\text{Co}_{0.08})_2\text{As}_2$  as a function of the polarization (see figures’s top). In all cases, the normalized intensities  $[\mu(E)]$  are presented. The open red circles in the insets of panels (b) and (e) show the difference spectrum  $[\mu(E)_{\phi=45} - \mu(E)_{\phi=0}]$  with the dashed lines marking some representative energy positions.

sample. Since this feature is well above the Fermi level, the composition effect is most likely due to the direct effect of the impurity scattering potential [50,51], and we conclude that Mn impurities act as stronger scattering centers than Co.

To estimate the composition effect in the edge intensity anisotropy as a function of  $\phi$   $[I(\phi)]$ , we adopt again the integrated areas of the edge features as the approximation to  $I(\phi)$ . This time, we undertake a direct approach numerically integrating the experimental data as exemplified in Fig. 5(a). Indeed, results from a line-shape analysis of the As  $K$  edge are too dependent on the choice of parameters, and we found that a numerical integration suffices to properly capture our results. For each  $\phi$ ,  $I(\phi)$  is obtained, and then the data are normalized as  $I(\phi)/I(\phi = 0)$ . Results for all samples are shown in Fig. 5(b). The error bars are estimated by small variations of the integration region. In comparison to the parent compound, the effect of Co substitution is clear, whereas that of Mn is weak but significant.

In Ref. [16], Co substitution is suggested to populate the As-derived orbitals. Here, we show that the electrons

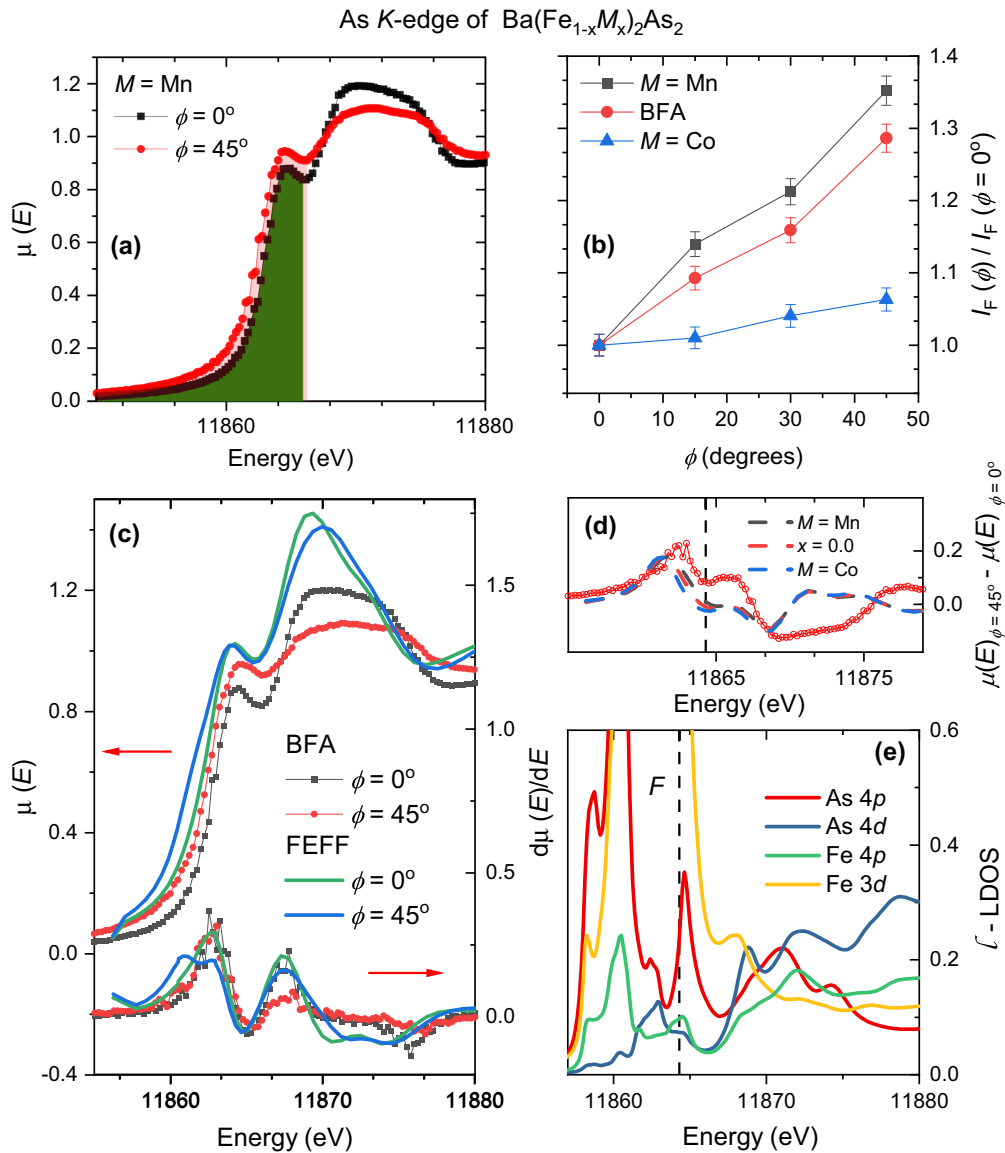


FIG. 5. (a) Normalized intensities  $[\mu(E)]$  of the As  $K$ -edge XANES spectra of  $\text{Ba}(\text{Fe}_{1.92}\text{Mn}_{0.08})_2\text{As}_2$  for  $\phi = 0$  and  $\phi = 45^\circ$ . In each case, the panel shows the spectrum region taken into consideration to perform the numerical integration that represents the  $F$ -feature intensity  $[I_F(\phi)]$ . (b) The polarization dependence of the  $F$ -peak intensity as a function of  $\phi$ , for all compositions. In (c), we present polarization-dependent FEFF calculations of the As  $K$ -edge spectra (left axis) and its derivative (right axis) compared to the respective experimental data. A shift of 1 eV and a broadening of 1.2 eV were considered in the calculations. In panel (d), we present the difference spectrum of the  $\text{BaFe}_2\text{As}_2$  data (open red circles) compared to FEFF calculations of  $\text{Ba}(\text{Fe}_{1-x}\text{M}_x)_2\text{As}_2$  with  $M = \text{Mn}$  or  $\text{Co}$  and  $x = 0.1$  (see the main text). (e) FEFF-calculated site and orbital projected LDOS of  $\text{BaFe}_2\text{As}_2$  focusing on the Fe- and As-derived electronic states.

derived from Co substitution go preferentially to the unoccupied As  $4p_z$  states, characterizing a distinct charge transfer anisotropy. By causing an electronic transfer to orbitals along the  $c$  axis, Co substitution unbalances the electron and hole contributions to the transport along this direction, increasing the incoherent scattering in this direction. We, thus, support the interpretation given in Ref. [52] to the observed  $\text{BaFe}_2\text{As}_2$  interplane resistivity anisotropy and its increase with Co substitution [52,53]. Moreover, our results provide a real-space picture of the evolving three-dimensional character of the  $\text{BaFe}_2\text{As}_2$  electronic structure as previously probed by angle-resolved photoemission spectroscopy (ARPES) [54].

On the other hand, no change in electronic filling can be invoked as a mechanism to the anisotropy increase caused by Mn substitution. As we will discuss, this effect is connected to the localization of the Fe-derived electronic states. Indeed, isoelectronic substitutions, as observed by resonant inelastic x-ray scattering experiments of Mn- and P-substituted  $\text{BaFe}_2\text{As}_2$  [36,55], may increase electronic correlations.

We performed polarization-dependent FEFF calculations, aiming at describing two effects: the spectra anisotropy and the composition dependence of this effect. In Fig. 5(c), we compare the experimental and calculated As  $K$  edges of  $\text{BaFe}_2\text{As}_2$  for  $\phi = 0$  and  $\phi = 45^\circ$  and their respective deriva-

TABLE I. Metal and ligand-orbital composition of the FeAs<sub>4</sub> ligand-field molecular orbitals. Numbers are given in percentages of normalized wave functions. The final orbital composition analysis was performed adopting the Ros-Schuit partition method via the MULTIFWN program [62].

Iron orbitals (MO symmetry) Ligand-field relative energies/eV		$3d_{z^2}$ ( $a_1^*$ ) 0.000	$3d_{xy}$ ( $b_2^*$ ) 0.002	$3d_{xz}, 3d_{yz}$ ( $e^*$ ) 0.260	$3d_{x^2-y^2}$ ( $b_1^*$ ) 0.308
Fe orbitals	$4p_z$			4.48	2.25
	$4p_y$ and $4p_x$	5.80		10.32	5.80
As orbitals	$4p_z$	2.75		2.00	2.38
	$4p_y$ and $4p_x$	0.89	4.15	7.79	5.80

tives. The overall spectral shape and anisotropy are well reproduced, but there is a lack of detail in the effect of the anisotropy. In the calculations, the edge peaks nearly coincide whereas, in the experiments, the edge intensity of the  $\phi = 45^\circ$  spectra sits above the  $\phi = 0$  spectra for all compositions.

To simulate the effects of chemical substitution, we performed FEFf calculations replacing one in ten Fe atoms with a dopant (either Mn or Co). This is equivalent to a  $x = 0.1$  composition, which is close to our samples for which  $x = 0.08$ . Three dopant distributions were calculated and then averaged out. In Fig. 5(d), we compare the difference spectrum [ $\mu(E)_{\phi=45} - \mu(E)_{\phi=0}$ ] obtained from the BaFe<sub>2</sub>As<sub>2</sub> data (open red circles) and from FEFf calculations of the parent compound and substituted samples (thick lines). As can be observed, the edge polarization dependence is partially reproduced, but only a small composition effect is observed in the FEFf calculations.

In Fig. 5(e), we show the site and orbital-projected LDOS obtained from FEFf calculations. The  $F$ -feature position is marked for comparison. It shows that the main edge is dominated by As  $4p$  states as expected. Moreover, the high density of Fe  $3d$  states about the edge position allows the formation of Fe  $3d$ As  $4p$  hybrid bands making the As  $K$ -edge transition sensitive to this mixing. The LDOS of the Fe  $4p$ -derived states also peaks about the  $F$  as also calculated in the case of the Fe  $K$  edge, further suggesting its relevance to the electronic states about the Fermi energy. Here, due to the As  $K$ -edge higher energy, core-hole effects are likely less relevant than for the Fe  $K$  edge, [see the inset of Fig. 3(e)], validating the present discussion in a first approximation.

Whereas our FEFf calculations for the Fe and As  $K$  edges are able to support our discussion of the experimental results, it is clear that some aspects of the physics of our system are not captured. This is nothing but an expression of the still unresolved character of the electronic states of the FePn materials, that lie in the border between strong and weak electronic correlations. We, thus, resort to quantum chemistry calculations of the electronic properties of a single FeAs<sub>4</sub>-distorted tetrahedron within a multiconfigurational calculation of the orbital states [32,33,41,42].

Because XANES is a local probe to electronic structure, it is reasonable to assume that the electronic structure of a single FeAs<sub>4</sub>-distorted tetrahedron can be connected to the preedge feature which, insofar as the Fe  $K$  edge is concerned, is the main focus of our paper. Our results are presented in Fig. 6 and in Table I. In doing that, we are assuming that the XANES transitions in our materials are mainly due to local processes, which excludes the metal-metal charge transfer

that is observed in certain transition-metal complexes [56,57]. One can justify this assumption based on the As chemistry, which tends to form complexes with a low bridging character with the As  $4p$  states well localized on the As sites. This orbital localization would weaken the Fe-Fe charge transfer that relies on the mediation of the ligand orbitals.

The multiconfigurational calculations results show that the first set of partially occupied states are, indeed, ligand-field (or crystal-field) levels formed by hybrid orbitals from Fe  $3d$  and As  $4p$  states. In our discussion, we name the  $|a_1^*$ ,  $|b_2^*$ ,  $|e^*$ , and  $|b_1^*$  molecular orbitals by their Fe  $3d$  main character, respectively,  $d_{z^2}$ ,  $d_{xy}$ ,  $d_{xz}/d_{yz}$ , and  $d_{x^2-y^2}$ . The calculated ligand-field splitting of only  $\approx 0.3$  eV is in qualitative agreement with previous calculations [58].

From Table I and from the isosurface plot of the molecular orbital (MO) wave functions in Fig. 6, one can observe that all  $d_{xy}$ ,  $d_{xz}/d_{yz}$ , and  $d_{x^2-y^2}$  hybridize with the As  $4p_{x,y,z}$  orbitals. The  $d_{z^2}$  and  $d_{xy}$  orbitals appear in our calculations as nearly degenerate states and are indicated to be virtually double occupied. Electronic transitions are, thus, dominated by the  $d_{xz}/d_{yz}$  and  $d_{x^2-y^2}$  hybrid orbitals.

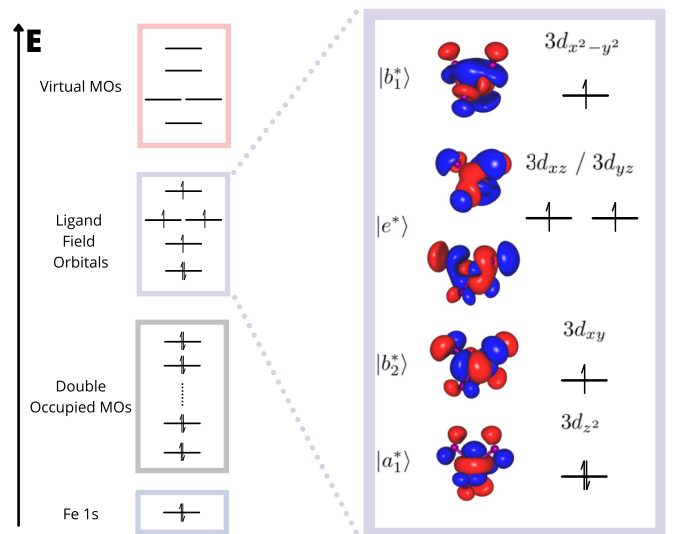


FIG. 6. Left panel: the energetic ordering of fully occupied, ligand field, and virtual orbitals as obtained from our calculations. Right panel: ligand-field molecular orbitals and their ground-state configurations based on the CAS(6,5)/NEVPT-2/Def2-TZVPP approach [41]. Isosurface values are set to 0.006. Our results indicate a ligand-field splitting of 0.308 eV. Ligand orbitals are plotted via the GABEDIT program [61].

All the  $d_{xz}/d_{yz}$  and  $d_{x^2-y^2}$  display contributions with  $p_z$ -orbital character and, therefore, contribute to the increase of the spectra intensity for  $\phi$  rotations. It should be noted that even if the  $d_{xy}$  orbital was not double occupied, it would not contribute to this since they present no mixing with  $p_z$  orbitals. The calculated hybridization pattern of the ligand-field orbitals is imposed by the specific properties of the  $\text{FeAs}_4$  complex. Indeed, the  $D_{2d}$  symmetry would allow the mixing of  $p_z$  orbitals into the  $d_{xy}$  orbital, whereas it would prevent any  $p_z$ -orbital mixing with  $d_{x^2-y^2}$ .

The most prominent feature to be observed from our calculations is the contribution from the Fe  $4p$  states to ligand-field orbitals, forming Fe  $3d4p$  hybrid states. This local  $pd$  hybridization is acquired by the Fe  $3d$  states as a formal way of reducing their antibonding character, which is implied by the  $\text{As}^{-3}-\pi$  donation. This effect is a mechanism for the localization of the Fe  $3d$  states as observed in other coordination complexes [59]. As a consequence, the preedge peak in the Fe  $K$  edge can be attributed to Fe  $3d4p$  hybridization in Fe complexes [60], and our findings propose that we should reconsider the nature of the preedge transition of the Fe  $K$  edge of the FePn materials. Indeed, so far in our discussion as well as in previous works [18,25–28], the contribution of the Fe  $4p$  states to the preedge was overlooked. We will argue that this local hybridization is key to understand the effects of Mn substitution.

First, we expect that via the Fe  $3d$  As  $4p$  mixing, the Fe  $K$ -edge results should mirror that of the As  $K$  edge as observed. This expectation, however, does not take into account that the preedge intensity may be dominated by transitions to the Fe  $3d4p$  states. This is likely the case of FeSe materials [29] for which the Se  $K$  edge clearly indicates that the Se  $4p_{x,y}$  planar orbitals dominate the density of unoccupied states, whereas the contrary is concluded from the Fe  $K$  edge.

Mn substitution may weak the Fe  $3d$  As  $4p$  mixing, making the Fe orbitals more localized through the mechanisms above explained. In turn, this would make the Fe  $3d4p_z$  mixing stronger, increasing the observed polarization dependence. In the same direction, the As  $4p$  will also become more localized, rendering the As  $K$  edge spectra more anisotropic. Both effects are observed in Figs. 3(b) and 5(b) and we propose that this is the mechanism related to Mn substitution in  $\text{BaFe}_2\text{As}_2$ : Mn impurities localize the Fe  $3d$  states by changing the Fe  $3d$  As  $4p$  mixing. In turn, it shows that hole doping is not the only active mechanism pushing  $\text{BaFe}_2\text{As}_2$  to a more correlated Mott phase.

#### IV. SUMMARY AND CONCLUSIONS

We have investigated the polarization dependence of the Fe and As  $K$ -edge XANES spectra of  $\text{BaFe}_2\text{As}_2$  and chemically substituted Mn and Co materials of this parent compound. In

the case of the Fe  $K$  edge, we focused our analysis on the transitions allowed by Fe  $3d$  As  $4p$  hybrid orbitals that span the preedge structure of the Fe  $K$ -edge spectra. In the case of the As  $K$  edge, we focused on the edge transitions, probing the As  $4p_{x,y,z}$  orbitals.

The polarization dependence indicates that Co substitution populates preferentially the hybrid bands with unoccupied states along the  $c$  axis ( $p_z$  orbitals) as concluded from the strong reduction of the As  $K$ -edge anisotropy. This is a distinct anisotropic charge-transfer effect, which may be connected to the transport properties and ARPES experiments of Co-doped  $\text{BaFe}_2\text{As}_2$  [52–54].

Mn substitution, whereas not changing the material electronic filling, increases the anisotropy of the probed electronic states. We attributed this finding to a delicate interplay between the local Fe  $3d4p$  and the metal-ligand Fe  $3d$  As  $4p$  mixings with Mn substitution favoring the Fe  $3d$  localization by hindering the Fe  $3d$  As  $4p$  mixing.

In all cases, the XANES polarization dependence revealed a higher density of an unoccupied state for orbitals with  $p_z$  character with the results from the Fe  $K$  edge mirroring those of the pnictide  $K$  edge. Our quantum chemistry calculations show this is not the only result that could be expected since the local Fe  $3d4p$  hybridization also contributes to the preedge transitions and may dominate its polarization dependence. This is likely the case of FeSe materials [29]. One can, thus, state a clear distinct behavior of the electronic states of iron arsenides and selenides with the former presenting a stronger Fe  $3d$  As  $4p$  hybridization, which favors the occupation of orbitals with planar geometry, whereas orbitals along the  $c$  axis remain unoccupied.

Overall, our findings suggest that the interplay between the local Fe  $3d4p$  and the metal-ligand Fe  $3d$  As(Se) $4p$  mixings is a common thread of the FePn electronic structure, unveiling the key role played by Fe  $4p$  states.

#### ACKNOWLEDGMENTS

We acknowledge CNPEM-LNLS for the concession of beamtime at the XDS beamline (Proposals No. 20180194 and No. 20190123). The XDS beamline staff is acknowledged for their assistance during the experiments. Fundação de Amparo à Pesquisa do Estado de São Paulo financial support is acknowledged by M.R.C. (Grants No. 2019/05150-7 and No. 2020/13701-0) W.R.S.N. (Grant No. 2019/23879-4), D.S.C. (Grant No. 2019/04196-3), J.C.S. (Grants No. 2018/11364-7 and No. 2020/12283-0), M.M.P. (Grant No. 2015/15665-3), P.G.P. and C.A. (Grant No. 2017/10581-1), and F.A.G. (Grant No. 2019/25665-1). P.G.P. and C.A. acknowledge financial support from CNPq: CNPq Grants No. 304496/2017-0 and CNPq No. 310373/2019-0.

- [1] Y. Kamihara, T. Watanabe, M. Hirano, and H. Hosono, *J. Am. Chem. Soc.* **130**, 3296 (2008).
- [2] H. Hosono and K. Kuroki, *Physica C* **514**, 399 (2015).
- [3] A. Chubukov, *Annu. Rev. Condens. Matter Phys.* **3**, 57 (2012).

- [4] L. de' Medici, G. Giovannetti, and M. Capone, *Phys. Rev. Lett.* **112**, 177001 (2014).
- [5] Z. P. Yin, K. Haule, and G. Kotliar, *Nat. Phys.* **7**, 294 (2011).
- [6] Z. P. Yin, K. Haule, and G. Kotliar, *Nature Mater.* **10**, 932 (2011).



- [7] A. S. Sefat, R. Jin, M. A. McGuire, B. C. Sales, D. J. Singh, and D. Mandrus, *Phys. Rev. Lett.* **101**, 117004 (2008).
- [8] J. S. Kim, S. Khim, H. J. Kim, M. J. Eom, J. M. Law, R. K. Kremer, J. H. Shim, and K. H. Kim, *Phys. Rev. B* **82**, 024510 (2010).
- [9] Y. Singh, A. Ellern, and D. C. Johnston, *Phys. Rev. B* **79**, 094519 (2009).
- [10] Y. Singh, M. A. Green, Q. Huang, A. Kreyssig, R. J. McQueeney, D. C. Johnston, and A. I. Goldman, *Phys. Rev. B* **80**, 100403(R) (2009).
- [11] A. S. Sefat, D. J. Singh, R. Jin, M. A. McGuire, B. C. Sales, and D. Mandrus, *Phys. Rev. B* **79**, 024512 (2009).
- [12] V. K. Anand, D. G. Quirinale, Y. Lee, B. N. Harmon, Y. Furukawa, V. V. Ogloblichev, A. Huq, D. L. Abernathy, P. W. Stephens, R. J. McQueeney, A. Kreyssig, A. I. Goldman, and D. C. Johnston, *Phys. Rev. B* **90**, 064517 (2014).
- [13] E. M. Bittar, C. Adriano, T. M. Garitezi, P. F. S. Rosa, L. Mendonça-Ferreira, F. Garcia, G. de M. Azevedo, P. G. Pagliuso, and E. Granado, *Phys. Rev. Lett.* **107**, 267402 (2011).
- [14] V. Balédent, F. Rullier-Albenque, D. Colson, G. Monaco, and J.-P. Rueff, *Phys. Rev. B* **86**, 235123 (2012).
- [15] M. Merz, F. Eilers, T. Wolf, P. Nagel, H. van Loehneysen, and S. Schuppler, *Phys. Rev. B* **86**, 104503 (2012).
- [16] V. Baledent, F. Rullier-Albenque, D. Colson, J. M. Ablett, and J.-P. Rueff, *Phys. Rev. Lett.* **114**, 177001 (2015).
- [17] H. Yamaoka, Y. Yamamoto, J.-F. Lin, J. J. Wu, X. Wang, C. Jin, M. Yoshida, S. Onari, S. Ishida, Y. Tsuchiya, N. Takeshita, N. Hiraoka, H. Ishii, K.-D. Tsuei, P. Chow, Y. Xiao, and J. Mizuki, *Phys. Rev. B* **96**, 085129 (2017).
- [18] J. Pellicciari, K. Ishii, L. Xing, X. Wang, C. Jin, and T. Schmitt, *Appl. Phys. Lett.* **118**, 112604 (2021).
- [19] E. Granado, L. Mendonça-Ferreira, F. Garcia, G. de M. Azevedo, G. Fabbris, E. M. Bittar, C. Adriano, T. M. Garitezi, P. F. S. Rosa, L. F. Bufaiçal, M. A. Avila, H. Terashita, and P. G. Pagliuso, *Phys. Rev. B* **83**, 184508 (2011).
- [20] J. Cheng, P. Dong, W. Xu, S. Liu, W. Chu, X. Chen, and Z. Wu, *J. Synchrotron Radiat.* **22**, 1030 (2015).
- [21] W. Chu, J. Cheng, S. Chu, T. Hu, A. Marcelli, X. Chen, and Z. Wu, *Sci. Rep.* **3**, 1750 (2013).
- [22] W. Xu, A. Marcelli, B. Joseph, A. Iadecola, W. S. Chu, D. Di Gioacchino, A. Bianconi, Z. Y. Wu, and N. L. Saini, *J. Phys.: Condens. Matter* **22**, 125701 (2010).
- [23] B. Joseph, A. Ricci, N. Poccia, V. G. Ivanov, A. A. Ivanov, A. P. Menushenkov, N. L. Saini, and A. Bianconi, *J. Supercond. Novel Magn.* **29**, 3041 (2016).
- [24] M. Y. Hacisalihoglu, E. Paris, B. Joseph, L. Simonelli, T. J. Sato, T. Mizokawa, and N. L. Saini, *Phys. Chem. Chem. Phys.* **18**, 9029 (2016).
- [25] S. Lafuerza, H. Gretarsson, F. Hardy, T. Wolf, C. Meingast, G. Giovannetti, M. Capone, A. S. Sefat, Y.-J. Kim, P. Glatzel, and L. de' Medici, *Phys. Rev. B* **96**, 045133 (2017).
- [26] C. L. Chen, S. M. Rao, C. L. Dong, J. L. Chen, T. W. Huang, B. H. Mok, M. C. Ling, W. C. Wang, C. L. Chang, T. S. Chan, J. F. Lee, J.-H. Guo, and M. K. Wu, *Europhys. Lett.* **93**, 47003 (2011).
- [27] C. L. Chen, C. L. Dong, J. L. Chen, J.-H. Guo, W. L. Yang, C. C. Hsu, K. W. Yeh, T. W. Huang, B. H. Mok, T. S. Chan, J. F. Lee, C. L. Chang, S. M. Rao, and M. K. Wu, *Phys. Chem. Chem. Phys.* **13**, 15666 (2011).
- [28] B. C. Chang, Y. B. You, T. J. Shiu, M. F. Tai, H. C. Ku, Y. Y. Hsu, L. Y. Jang, J. F. Lee, Z. Wei, K. Q. Ruan, and X. G. Li, *Phys. Rev. B* **80**, 165108 (2009).
- [29] B. Joseph, A. Iadecola, L. Simonelli, Y. Mizuguchi, Y. Takano, T. Mizokawa, and N. L. Saini, *J. Phys.: Condens. Matter* **22**, 485702 (2010).
- [30] S. I. Zabinsky, J. J. Rehr, A. Ankudinov, R. C. Albers, and M. J. Eller, *Phys. Rev. B* **52**, 2995 (1995).
- [31] J. J. Rehr and R. C. Albers, *Rev. Mod. Phys.* **72**, 621 (2000).
- [32] F. Neese, *WIREs Comput. Mol. Sci.* **2**, 73 (2012).
- [33] F. Neese, *WIREs Comput. Mol. Sci.* **8**, e1327 (2018).
- [34] T. M. Garitezi, C. Adriano, P. F. S. Rosa, E. M. Bittar, L. Bufaiçal, R. L. d. Almeida, E. Granado, T. Grant, Z. Fisk, M. A. Avila, R. A. Ribeiro, P. L. Kuhns, A. P. Reyes, R. R. Urbano, and P. G. Pagliuso, *Braz. J. Phys.* **43**, 223 (2013).
- [35] A. Thaler, H. Hodovanets, M. S. Torikachvili, S. Ran, A. Kracher, W. Straszheim, J. Q. Yan, E. Mun, and P. C. Canfield, *Phys. Rev. B* **84**, 144528 (2011).
- [36] F. A. Garcia, O. Ivashko, D. E. McNally, L. Das, M. M. Piva, C. Adriano, P. G. Pagliuso, J. Chang, T. Schmitt, and C. Monney, *Phys. Rev. B* **99**, 115118 (2019).
- [37] P. F. S. Rosa, C. Adriano, T. M. Garitezi, M. M. Piva, K. Mydeen, T. Grant, Z. Fisk, M. Nicklas, R. R. Urbano, R. M. Fernandes, and P. G. Pagliuso, *Sci. Rep.* **4**, 6252 (2014).
- [38] F. A. Lima, M. E. Saleta, R. J. S. Pagliuca, M. A. Eleotério, R. D. Reis, J. Fonseca Júnior, B. Meyer, E. M. Bittar, N. M. Souza-Neto, and E. Granado, *J. Synchrotron Radiat.* **23**, 1538 (2016).
- [39] B. Ravel and M. Newville, *J. Synchrotron Radiat.* **12**, 537 (2005).
- [40] L. Hedin and B. I. Lundqvist, *J. Phys. C* **4**, 2064 (1971).
- [41] S. K. Singh, J. Eng, M. Atanasov, and F. Neese, *Coord. Chem. Rev.* **344**, 2 (2017).
- [42] P. Norman and A. Dreuw, *Chem. Rev.* **118**, 7208 (2018).
- [43] F. d. Groot, G. Vankó, and P. Glatzel, *J. Phys.: Condens. Matter* **21**, 104207 (2009).
- [44] G. Vankó, F. M. F. de Groot, S. Huotari, R. J. Cava, T. Lorenz, and M. Reuther, [arXiv:0802.2744](https://arxiv.org/abs/0802.2744).
- [45] J. Stöhr and H. C. Siegmann, *Magnetism: From Fundamentals to Nanoscale Dynamics* (Springer-Verlag, Berlin/Heidelberg, 2006).
- [46] B. Mounsséf, M. R. Cantarino, E. M. Bittar, T. M. Germano, A. Leithe-Jasper, and F. A. Garcia, *Phys. Rev. B* **99**, 035152 (2019).
- [47] H. Suzuki, T. Yoshida, S. Ideta, G. Shibata, K. Ishigami, T. Kadono, A. Fujimori, M. Hashimoto, D. H. Lu, Z.-X. Shen, K. Ono, E. Sakai, H. Kumigashira, M. Matsuo, and T. Sasagawa, *Phys. Rev. B* **88**, 100501(R) (2013).
- [48] Y. Texier, Y. Laplace, P. Mendels, J. T. Park, G. Friemel, D. L. Sun, D. S. Inosov, C. T. Lin, and J. Bobroff, *Europhys. Lett.* **99**, 17002 (2012).
- [49] A. L. Ankudinov, B. Ravel, J. J. Rehr, and S. D. Conradson, *Phys. Rev. B* **58**, 7565 (1998).
- [50] T. Kobayashi, M. Nakajima, S. Miyasaka, and S. Tajima, *Phys. Rev. B* **94**, 224516 (2016).
- [51] M. Merz, P. Schweiss, P. Nagel, M.-J. Huang, R. Eder, T. Wolf, H. von Loehneysen, and S. Schuppler, *J. Phys. Soc. Jpn.* **85**, 044707 (2016).

- [52] M. Nakajima, M. Nagafuchi, and S. Tajima, *Phys. Rev. B* **97**, 094511 (2018).
- [53] M. A. Tanatar, N. Ni, A. Thaler, S. L. Bud'ko, P. C. Canfield, and R. Prozorov, *Phys. Rev. B* **84**, 014519 (2011).
- [54] S. Thirupathaiah, S. de Jong, R. Ovsyannikov, H. A. Dürr, A. Varykhalov, R. Follath, Y. Huang, R. Huisman, M. S. Golden, Y.-Z. Zhang, H. O. Jeschke, R. Valentí, A. Erb, A. Gloskovskii, and J. Fink, *Phys. Rev. B* **81**, 104512 (2010).
- [55] J. Pelliciari, K. Ishii, Y. Huang, M. Dantz, X. Lu, P. Olalde-Velasco, V. N. Strocov, S. Kasahara, L. Xing, X. Wang, C. Jin, Y. Matsuda, T. Shibauchi, T. Das, and T. Schmitt, *Commun. Phys.* **2**, 139 (2019).
- [56] C. Gougoussis, M. Calandra, A. Seitsonen, C. Brouder, A. Shukla, and F. Mauri, *Phys. Rev. B* **79**, 045118 (2009).
- [57] D. Cabaret, A. Bordage, A. Juhin, M. Arfaoui, and E. Gaudry, *Phys. Chem. Chem. Phys.* **12**, 5619 (2010).
- [58] K. Haule and G. Kotliar, *New J. Phys.* **11**, 025021 (2009).
- [59] S. Alvarez and J. Cirera, *Angew. Chem., Int. Ed.* **45**, 3012 (2006).
- [60] R. K. Hocking and E. I. Solomon, *Ligand Field and Molecular Orbital Theories of Transition Metal X-ray Absorption Edge Transitions* (Springer, Berlin/Heidelberg, 2012), pp. 155–184.
- [61] A.-R. Allouche, *J. Comput. Chem.* **32**, 174 (2011).
- [62] T. Lu and F. Chen, *J. Comput. Chem.* **33**, 580 (2012).